Structural Engineering and Mechanics, Vol. 40, No. 3 (2011) 297-313
DOI: http://dx.doi.org/10.12989/sem.2011.40.3.297

A method for evaluation of longitudinal joint connections of decked precast concrete girder bridges

Matthew Z. Smith[a], Yue Li* and William M. Bulleit[b]

Department of Civil and Environmental Engineering, Michigan Technological University, 1400 Townsend Dr., Houghton, MI 49931-1295, USA

(Received August 30, 2009, Revised April 9, 2011, Accepted August 17, 2011)

Abstract. As bridge conditions in the United States continue to deteriorate, rapid bridge replacement procedures are needed. Decked precast prestressed concrete (DPPC) girders are used for rapid bridge construction because the bridge deck is precast with the girders eliminating the need for a cast-in-place slab. One of the concerns with using DPPC girders as a bridge construction option is the durability of the longitudinal joints between girders. The objectives of this paper were to propose a method to use a spring element modeling procedure for representing welded steel connector assemblies between adjacent girders in DPPC girder bridges, perform a preliminary study of bridge performance under multiple loading scenarios and bridge configurations, and discuss model flexibility for accommodating future field data for model verification. The spring elements have potential to represent the contribution of joint grout materials by altering the spring stiffness.

Keywords: bridges; concrete; finite element model; spring elements; welded shear connectors

1. Introduction

The transportation infrastructure in the United States continues to deteriorate, including the bridges that help the infrastructure span rivers and valleys. The transportation infrastructure is the biggest investment in the United States with an estimated value of $20 trillion. In 2009, the American Society of Civil Engineers (ASCE) gave a report card grade of C for bridge conditions throughout the United States (ASCE 2009). More than 26% of the nation's bridges are either structurally deficient or functionally obsolete. A $17 billion annual investment is needed to substantially improve current bridge conditions. Currently, only $10.5 billion is spent annually on the construction and maintenance of bridges (ASCE 2009). Many of these existing bridges will need replacement now or in the future resulting in lengthy bridge construction procedures. These construction procedures can create unwanted detours and unsafe construction sites. Rapid bridge construction methods need more consideration in this fast-paced world.

One option for bridge replacement is decked precast prestressed concrete (DPPC) girders, which

*Corresponding author, Associate Professor, E-mail: yueli@mtu.edu
[a]Formerly, Graduate Student, E-mail: mzsmith@mtu.edu
[b]Professor, E-mail: wmbullei@mtu.edu

allow staged and rapid bridge construction. DPPC girders usually consist of a typical I-shape girder or box beam topped with a portion of the deck at the precast plant before delivery to the construction site. The added deck eliminates the need for a cast-in-place slab creating a rapid bridge construction process. The added deck acts as an additional flange resulting in added stiffness for the girder. In addition, DPPC girders address sustainability issues by reducing detours, which reduces fuel consumption, and these girders are precast in a controlled environment which improves the girder quality and bridge life.

DPPC girders span farther than un-topped girders with unsupported lengths of 37-46 meters (120-150 feet). Upon delivery the girders are placed on the abutments. Steel or concrete diaphragms are installed at intermediate points along the length of the bridge to help distribute loads between girders. The DPPC girders can be connected longitudinally with shear connectors welded to concrete embedded angles (or transverse post-tensioning) and grouted shear keys between adjacent girder deck flanges. The most common material used to fill the shear keys in adjacent member bridges is a non-shrink cement grout (PCI 2007). A wearing surface is then added completing the bridge construction process.

Welded shear connectors consist of embedded angles in adjacent girders connected with a welded steel plate. Two headed studs are welded to the angles to allow for proper anchorage into the concrete girder flange (PCI 2007). This connection type currently does not have any design method published (Gergely *et al.* 2007). The designs for joints and connections between adjacent girders have been limited to rule-of-thumb methods and past experience creating a variety of welded plate connector spacing and keyway geometries in states that use these bridges (Chaudhury and Ma 2004).

DPPC girders have been used in areas where fresh concrete is difficult to obtain, in areas with relatively low traffic, and in areas with a short construction season (Hieber *et al.* 2005). The biggest concern when using DPPC girders for bridge construction is the durability of the longitudinal joints between adjacent girders. The Washington State Department of Transportation (WSDOT) has seen cracking in the overlay over the longitudinal joints of many prestressed multi-beam concrete bridges, often running the length of the bridge (Hieber *et al.* 2005). These cracks allow leakage to occur through the joints, which allows deicers to penetrate to the girders. Breakdown in the connections could result in significant damage to the bridge, which leads to a limited use of DPPC girders in areas such as the State of Michigan where deicers are commonly used on roads in the winter.

Jones and Boaz (1986) generated a governing system of equations for modeling an entire bridge system consisting of individual double tee girders connected with spring elements along the longitudinal joints. They found that as the number of spring element connections increased between adjacent girders (along the longitudinal joint), the more the bridge responded as though the longitudinal joint was continuously connected. It was also shown that individual discrete connections can develop large forces in this type of bridge.

Millam and Ma (2005) modeled the longitudinal joint connections between DPPC girders as two extreme conditions, fixed or hinged. The fixed joint acts like a cast-in-place slab transferring all transverse moment between adjacent girders, while the hinged joint connection transfers zero moment between adjacent girders. Both connections transferred all shear and transverse axial force. Pipkorn (2006) also modeled the longitudinal joint connections as fixed or hinged using master/slave node constraints. Right (non-skew) bridge geometries were considered to investigate joint behavior and bridge deflection trends.

Ma *et al.* (2007) summarized field-testing of eight decked bulb-tee girder bridges as well as development of three-dimensional finite element (FE) models. Using calibrated 3D FE models, parametric studies were performed to examine the effect of shear connectors and intermediate diaphragms on live-load distribution and connector forces. In the 3D FE model, 2-node hinge-connector elements were used to model shear connectors, and 3D truss elements were used to model intermediate steel diaphragms.

The main goal of this paper, which is based on a prior study by Smith (2007), was to determine the feasibility for modeling the welded shear connector assemblies using spring elements to represent the contribution of the assemblies and consider DPPC girder bridge models with skewed geometries. The research objectives were to propose a modeling procedure for representing steel connector assemblies between adjacent girders in DPPC girder bridges, perform a study of performance of bridge models under multiple loading scenarios and bridge configurations, and discuss model flexibility for accommodating future field data for model verification.

Due to the unavailability of data for DPPC girder bridge construction in Michigan, the authors were unable to verify results with a physical entity. However, verification and refinement of the models proposed should be included in future work when data is available.

2. Finite element bridge model

An AASHTO Type III girder pretopped with a 229-mm (9-in) deep by 2.235-m (7-ft 4-in) wide portion of the deck shown in Fig. 1 was used to illustrate the feasibility of the proposed method. Seven DPPC girders (Fig. 1) shown in Fig. 2 (with six longitudinal joints) were used in a two lane bridge with 3.658-m (12-ft) wide lanes, and shoulder width requirements and Type 4 barriers per Michigan Department of Transportation (MDOT) Bridge Design Guide (2005) requirements. The bridge measures 30.48-m (100-ft) in length and 15.65-m (51-ft 4-in) in width. All right bridge models were developed by Pipkorn (2006) and adjustments for shear connectors and skew were made in this research.

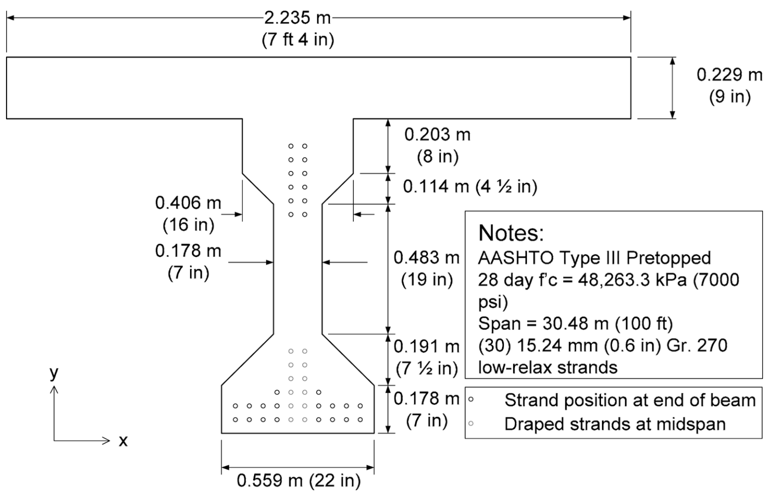

Fig. 1 Decked precast prestressed concrete girder

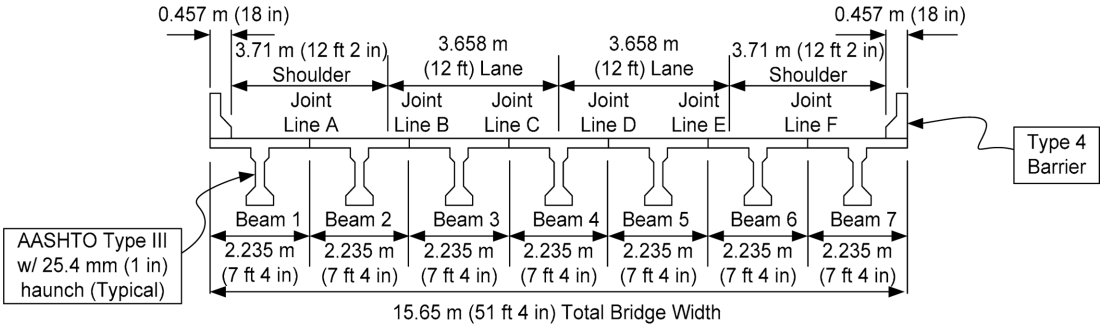

Fig. 2 Bridge cross-section (Pipkorn 2006)

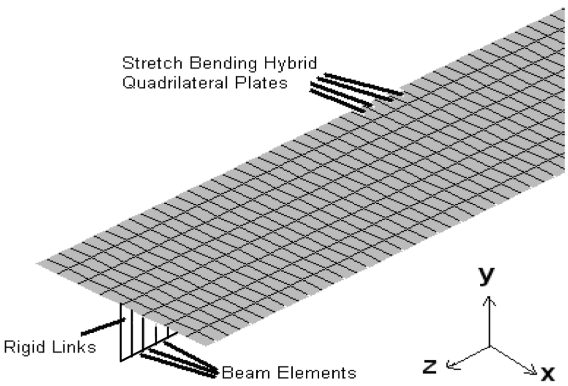

Fig. 3 Finite element composite girder (Pipkorn 2006)

PSBeam (2000), a software package used by practicing engineers and a good tool for the finite element girder model calibration, was used to develop a strand pattern for the AASHTO Type III DPPC girder to meet allowable and ultimate flexural stress limitations (Pipkorn 2006). The girders did not have debonded or top strands, but strands were draped where needed to stay within allowable stress limits.

The finite element bridge model in this paper was constructed using finite element software GTStrudl 29 (2006). The behaviors of the individual composite girder, shown in Fig. 3, modeled in PSBeam (2000) and GTStrudl 29 (2006) were found to be comparable. In the model developed in GTStrudl, the individual non-composite girder was modeled using beam elements parallel to the global z-axis with properties specific to the AASHTO Type III girder. The concrete deck was modeled using stretching bending hybrid quadrilateral (SBHQ) plate elements. The rigid links created the required composite action between the non-composite girder (beam elements) and the deck (SBHQ plate elements). The torsional constant was developed using St. Venant's equation (Boresi and Schmidt 2002). The girder was broken up into individual sections with the torsion calculated for each section. The torsion for the girder is the sum of the torsions of each section.

For the finite element bridge model boundary conditions, it was assumed that one end of the bridge would be modeled as pinned with restraint in the global x, y and z directions. The other end was modeled as a roller with restraint only in the global x and y directions.

Diaphragms (single steel channel, MC 18×42.7, shown in Fig. 4) were modeled using beam

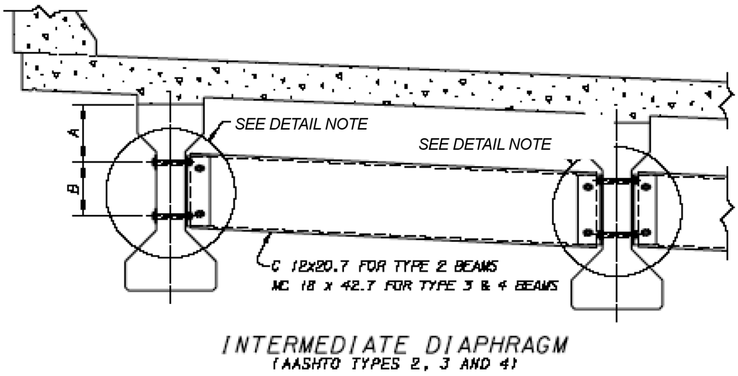

Fig. 4 MC18 × 42.7 intermediate diaphragm configuration

elements spaced at mid-span or 1/3 points along the length of the bridge model with no diaphragms located at the supports. The boundary conditions at each support accounted for lateral support in the global *x*-direction. These diaphragms typically take less time to install making them a good choice for the rapidly constructed bridges modeled in this research. Note that Fig. 4 is for illustration purposes only and is not representative of the deck modeled in this article. The flexibility of the bolted diaphragm-to-girder connection was not taken into account. Bridge geometries include right and skewed 15° through 30° at 5° increments. Diaphragms in the skewed bridge geometries were parallel with the support.

2.1 Load modeling

Four load cases were developed based upon the HL-93 AASHTO LRFD design truck from the AASHTO LRFD Bridge Design Specifications (2006). These four load cases are denoted M1, M2, V1, and V2. M1 and M2 load cases had one and two HL-93 trucks, respectively, located near mid-span to induce maximum moment. V1 and V2 load cases had one and two trucks, respectively, located near the supports to induce maximum shear. The M2 load case is shown in Fig. 5. The HL-93 design truck consists of a front axle load of 35.59 kN (8 kips) with intermediate and rear axle loads of 142.34 kN (32 kips) each. A uniform lane load of 9.34 kN/m (0.64 kips/ft) was applied evenly over a ten foot wide transverse strip. Other loads included in the load cases are the weight of the slabs and girders, the dead load of the barriers on each side of the bridge, and the prestressing forces applied to the composite girders. The finite element model was limited to static load conditions.

The prestressing was applied to the beam elements as a series of nodal loads equivalent to the total prestressing force in service, accounting for all prestress losses. Horizontal forces were applied to the beam element nodes within the transfer length zone until full prestress compression was achieved. The bending component of the prestressing inside the transfer length zone was created by the application of moments to the beam element nodes. The moments within the transfer length zone are equal to the sum of the prestressing force at the node in the transfer length zone times the eccentricity between the center of gravity of the non-composite girder and the changing center of gravity of the strand pattern minus the applied moment from the previous beam element node. Additional bending was also applied to the beam element nodes along the portion of the beam

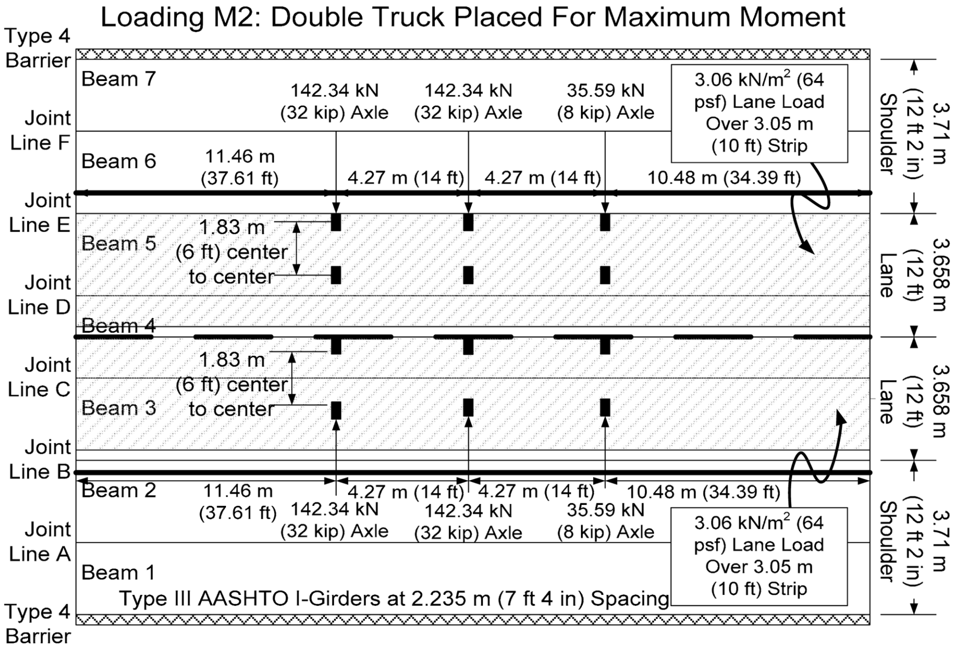

Fig. 5 M2 load case – plan view

outside the transfer length zone, which is equal to the total prestress force times the change in the center of gravity of the strand pattern (Pipkorn 2006).

The preliminary results summarized in the sections that follow are based on bridge models subjected to the M2 load case because the M2 load case typically produced the largest bridge deflections, largest forces and moments in the spring elements, and largest live load transverse distribution factors (based on moment).

2.2 Spring elements

2.2.1 Linear elastic behavior

The study of bridge performance for the bridge illustrated in Fig. 2 was conducted with four different spring element types representing one welded shear connector (steel plate). The connectors were spaced at either 0.61-m (2-ft) or 1.52-m (5-ft) along the longitudinal joints between adjacent girders. The spring elements provide four different stiffnesses: transverse axial, transverse moment, vertical shear, and horizontal shear with an elastic-plastic capability described subsequently.

The stiffnesses of the welded shear connector configuration shown in Fig. 6 are based on the stiffness of the A36 steel plate. All four spring elements for each individual plate are placed between the same two nodes, one node from each adjacent SBHQ plate element (composite girder flange) as shown in Fig. 7. Note that Fig. 7 is for illustration purposes only and that all four spring elements for each A36 steel plate are attached to the same two nodes A and B.

Two different A36 steel plates were modeled using elastic-plastic spring elements for this research. The plate sizes are 101.6-mm × 76.2-mm × 12.7-mm (4-in × 3-in × 1/2-in) and 152.4-mm × 101.6-mm × 19.1-mm (6-in × 4-in × 3/4-in).

In order to calculate the four different spring stiffnesses (i.e., transverse axial, transverse moment,

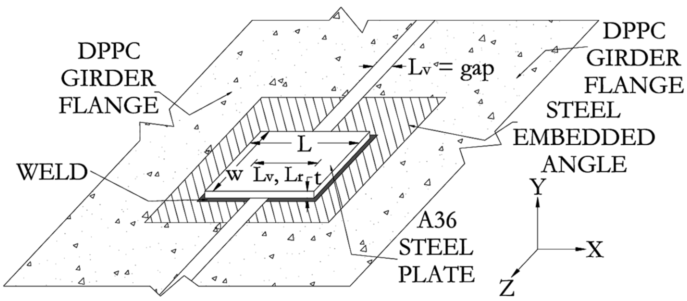

Fig. 6 Welded shear connector (A36 Steel)

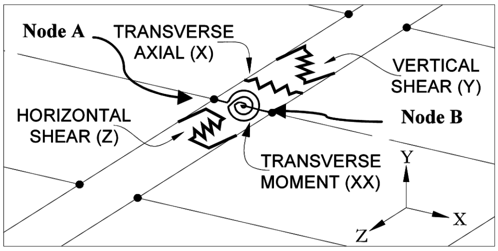

Fig. 7 Spring element modeling for weld shear connections

vertical shear, and horizontal shear) for use in the GTStrudl 29 (2006) bridge model, the following stiffness equations are used. Eq. (1) is used for axial stiffness of a member and is the transverse axial stiffness of the plate in units of force per length.

$$k_a = \frac{A \cdot E}{L_a} \tag{1}$$

where

A = cross-sectional area of the plate = $w \bullet t$ (from Fig. 6)
E = modulus of elasticity of the steel plate =200 GPa (29,000 ksi)
$L_a = L$ = length of plate parallel to force direction (shown in Fig. 6)

The vertical and horizontal shear stiffness is calculated based on Eq. (2), which is a virtual work equation used to solve for displacements in beams subjected to shear forces. Eq. (2) is integrated and solved for Eq. (3) assuming constant shear and unit deflection. Eq. (3) is used to calculate the vertical and horizontal shear stiffness with units of force per length.

$$\Delta = \int_0^L \frac{f_s \cdot V \cdot v}{A \cdot G} ds \tag{2}$$

where

f_s = size factor = 6/5 for rectangular cross-section
$V = F$ = actual applied shear force
v = 1 = unitless dummy load applied at desired location of deflection
A = cross-sectional area of the plate = $w \bullet t$
G = shear modulus of steel = 79.3 GPa

$$k_V = \frac{A \cdot G}{L_V \cdot f_s} \tag{3}$$

In Eq. (3), L_v = the length of the shear zone acted upon by the shear force. For horizontal shear, the shear zone is assumed to be the portion of the plate that exists over the gap (refer to Fig. 6). For vertical shear, the shear zone is the portion of the plate that exists between the centroid of welds on right side of the gap and the centroid of welds on left side of the gap (refer to Fig. 6).

In order to determine the transverse moment stiffness, Eq. (4) is used, which is a rotational stiffness and gives results in units of moment per rotation. Further discussion on the stiffness is presented in the section of effects of rotational stiffness.

$$k_r = \frac{4 \cdot E \cdot I}{L_r} \tag{4}$$

where

E = modulus of elasticity of the steel plate = 200 GPa (29,000 ksi)

I = moment of inertia of cross-section

L_r = half the distance from centroid of welds on right side of gap to centroid of welds on left side of gap (refer to Fig. 6)

2.2.2 Elastic plastic behavior

The yield force or moment and yield displacement or rotation is determined based on the 248 MPa (36 ksi) yield stress of A36 steel. Eq. (5) is used to determine the axial or shear force (F_v = 0.6 * F_y is the approximate yield shear stress used for this research) needed to yield the steel plate, and Eq. (6) is derived from Eq. (1) to calculate the change in length of the plate necessary to yield the plate. Eq. (7) is then used to calculate the moment needed to yield the plate, and Eq. (8) is used to calculate the yielding rotation for the plate.

$$P_y = F_y \cdot A \tag{5}$$

where

P_y = yield force

F_y = yield stress for A36 steel = 248 MPa (36 ksi)

A = cross-sectional area of the plate the force is acting over

$$\Delta L_y = \left(\frac{P_y}{A \cdot E}\right) \cdot L \tag{6}$$

where

A = cross-sectional area of the plate the force is acting over

E = modulus of elasticity of steel

L = L_a or L_v as appropriate (L_a for transverse axial stiffness and L_v for shear stiffnesses)

$$M_y = F_y \cdot S \tag{7}$$

where

F_y = yield stress for A36 steel = 248 MPa (36 ksi)

S = section modulus of the plate

$$\theta_y = \frac{M_y \cdot L}{E \cdot I} \tag{8}$$

where
M_y = yield moment
I = moment of inertia of plate
E = modulus of elasticity of steel
L = length of the plate

The hinged end plate, i.e., no rotational stiffness at either end, was created for comparison with the transverse moment stress from the plates modeled using two different transverse moment stiffnesses. The steel plate measures 101.6-mm × 76.2-mm × 12.7-mm (4-in × 3-in × 1/2-in) and has spring elements in the transverse axial, vertical shear, and horizontal shear directions.

Once the parameters were determined, the elastic-plastic curves were placed into the GTStrudl 29 (2006) models using macros, which were used for all large and repetitive tasks in the analysis.

3. Finite element analysis results

Both skew and right bridge models were subjected to the four load cases discussed previously for the preliminary study. The skew angles are 15°, 20°, 25°, and 30° with connector spacing at either 0.61-m (2-ft) or 1.52-m (5-ft). Finite element analysis results, including joint connection behavior, effects of connector spacing, effects of rotational rigidity, effects of skew angle, bridge deflections, and live load distribution factor for moment are discussed in the following sections.

The transverse moment stress is discussed for the effects of skew angle, the effects of connector spacing, and the effects of rotational stiffness. The transverse axial stress and the vertical shear stress are discussed for the effects of connector size and the horizontal shear stress was discussed for the effects of diaphragms.

3.1 Welded shear connector behavior

3.1.1 Effects of skew angle

The spring element forces and moments discussed below are for the M2 load case. Fig. 8 shows transverse moment stresses for the 101.6-mm × 76.2-mm × 12.7-mm steel plates. The skew and right bridges have one diaphragm at mid-span and spring elements spaced at 0.61-m (2-ft). The spring elements along joint line D are located between Beam 4 and 5, see Fig. 2 and Fig. 5.

The peaks in the stress curves shown in Fig. 8 are due to the location of the axle loads. The 142.34 kN (32 kip) axle loads from the HL-93 truck are located at the 11.58-m (38-ft) and 15.85-m (52-ft) locations. The smaller 35.59 kN (8 kip) axle load is located at the 20.12-m (66-ft) location. The largest transverse moment stresses are observed under the axle loads. When considering skew, it can be seen that as the skew angle increases, the transverse moment stress values in the welded shear connectors increase. The yielding stress of 248,200 kPa (36 ksi) for A36 steel has not been reached for these steel plates. The maximum transverse moment stress of 200 GPa (29 ksi) (80% of yielding stress) occurs at the 11.58-m (38-ft) location for the bridge with 30° of skew.

3.1.2 Effects of connector spacing

Chaudhury and Ma (2004) found that the designs for joints and connections between adjacent girders have been limited to rule-of-thumb methods and past experience. This lack of a design procedure has created a variety of welded plate connector spacing mostly based on empirical experience. This study examines the effects of different connector spacing on joint performance.

Fig. 9 shows transverse moment results for bridge geometries of right, 15º, 20º, 25º, and 30º skew with one diaphragm at mid-span, but the spring element spacing (welded shear connector spacing) is 1.52-m (5-ft) instead of 0.61-m (2-ft). Fig. 9 shows the transverse moment stress in the 101.6-mm × 76.2-mm × 12.7-mm steel plates along joint line D in Fig. 2 and Fig. 5.

Fig. 9 shows that the spring elements spaced at 1.52-m (5-ft) also transfer positive transverse moment similar to the spring elements spaced at 0.61-m (2-ft) in Fig. 8. Shifts in the stresses occur at the location of the axle loads in Fig. 9, but they are not as noticeable because a spring element does not exist at the axle load locations of 11.58-m (38-ft), 15.85-m (52-ft), and 20.12-m (66-ft) due to the 1.52-m (5-ft) spacing. The yielding stress has also not been reached with the 1.52-m (5-ft) spacing and the largest transverse moment stress occurs at the 12.19-m (40-ft) location with a value of 213.7 MPa (31 ksi) or 86% of the yielding stress. Comparing Fig. 9 to Fig. 8, it can be seen that the steel plates spaced at 1.52-m (5-ft) exhibit approximately 6.5% more transverse moment stress than the steel plates spaced at 0.61-m (2-ft).

3.1.3 Effects of connector size

The transverse axial and vertical shear stresses in the 101.6-mm × 76.2-mm ×12.7-mm and 152.4-mm ×101.6-mm ×19.1-mm steel plates will be compared to examine the effects of the steel plate size. The bridge models considered have 0.61-m (2-ft) spacing for the spring elements with one diaphragm at mid-span. The transverse axial and vertical shear stresses were taken from joint line D seen in Fig. 2 and Fig. 5.

Examining Fig. 10 shows the transverse axial stress in the 101.6-mm × 76.2-mm × 12.7-mm steel plates. Notice the transverse axial stress values peak at the 10-m (32.8-ft) location along the length of the bridge. This is close to the location of the rear axle load of 142.34 kN (32 kips) which was placed at the 11.58-m (38-ft) location. The positive transverse axial stress in this location signifies that the plates (spring elements) are in tension, meaning that Beam 4 and 5 (refer to Fig. 2) are trying to pull apart. A trend that can be seen in the data at the 10-m (32.8-ft) location is that as the

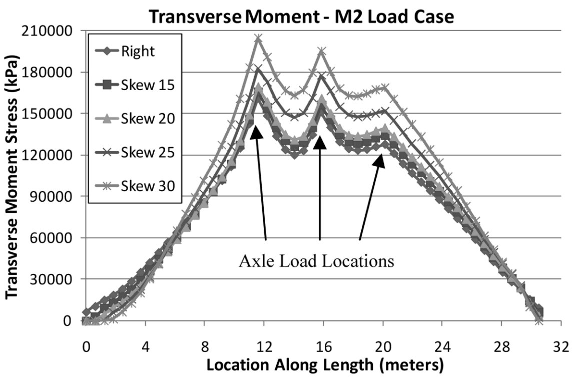

Fig. 8 Transverse moment stress (0.61-m (2-ft) spacing)

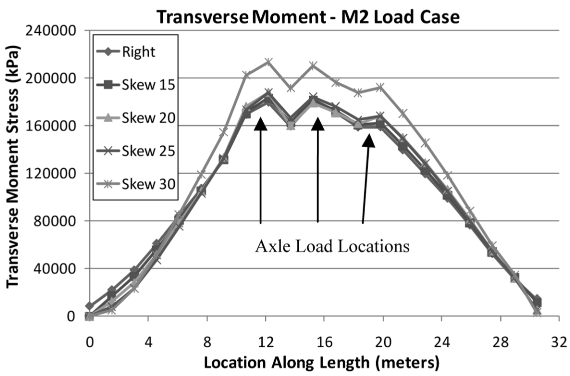

Fig. 9 Transverse moment stress (1.52-m (5-ft) spacing)

skew angle increases, so does the transverse axial stress. Notice that the same peak does not exist at the 15.85-m (52-ft) location of the intermediate 142.34 kN (32 kips) axle load. This is likely due to the diaphragm located at mid-span. The diaphragm prevents the truck loads from separating Beam 4 and 5 (refer to Fig. 2). To make sure that the mid-span diaphragm was causing the lack of transverse axial stress in the steel plates at the intermediate axle load location, transverse axial stresses were plotted from joint line D of the same bridge model configuration in Fig. 10, except no diaphragms were used. This analysis will be discussed subsequently.

Fig. 10 demonstrates that the 101.6-mm ×76.2-mm ×12.7-mm steel plates located at zero meters and 30.48-m (100-ft) along the length of the bridge have large transverse axial stress values compared to the rest of the steel plates throughout joint line D due to the supports not allowing girder movement in the transverse axial direction. A trend that can be seen at these end plate locations is that as the skew angle increases, the transverse axial stress decreases. Fig. 10 also shows a large number of steel plates have zero transverse axial stress since none of the load cases considered lateral loads. The largest transverse axial stress is seen in the steel plate for the right bridge geometry at the 30.48-m (100-ft) location with a stress value of 23 MPa (3.34 ksi). This stress value is well below the yield stress of A36 steel.

Comparing Fig. 11 to Fig. 10 shows that the larger steel plates have limited effect on the amount of transverse axial stress that is transferred over joint line D. Fig. 11 and Fig. 10 are almost identical in terms of transverse axial stresses in the steel plates.

The biggest difference between Fig. 11 and Fig. 10 can be seen at the zero meters and 30.48-m (100-ft) locations. Slightly larger transverse axial stresses can be seen in the 152.4-mm × 101.6-mm × 19.1-mm steel plates from Fig. 11 because these steel plates are larger than the 101.6-mm × 76.2-mm × 12.7-mm steel plates from Fig. 10. The stiffer plate transfers more load.

In Fig. 11, the largest transverse axial stress is seen in the steel plate for the right bridge geometry at the 30.48-m (100-ft) location with a stress value of 24.8 MPa (3.59 ksi). This stress value is well below the yield stress of A36 steel.

Fig. 12 was plotted for comparison to Fig. 10 to show the effects if no diaphragms were included in the bridge model. Notice in Fig. 12 that the lack of a diaphragm at mid-span has increased the transverse axial stress in the plates by a factor of 2.5 and the peak for the stresses is shifted toward mid-span when comparing to Fig. 10. Even a single diaphragm at mid-span has a significant effect on the transverse behavior of the connectors.

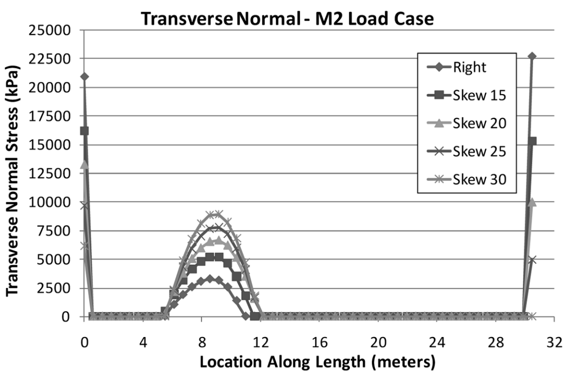

Fig. 10 Transverse axial stress (101.6-mm × 76.2-mm × 12.7-mm, one diaphragm)

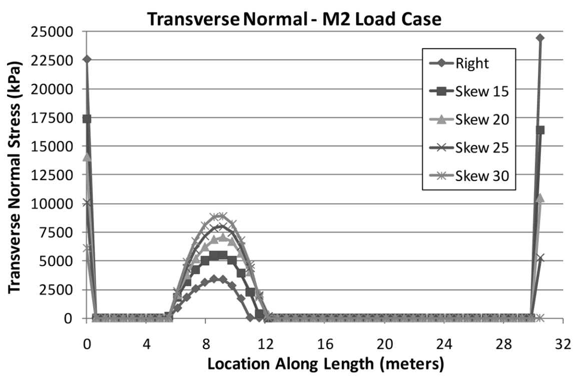

Fig. 11 Transverse axial stress (152.4-mm × 101.6-mm × 19.1-mm, one diaphragm)

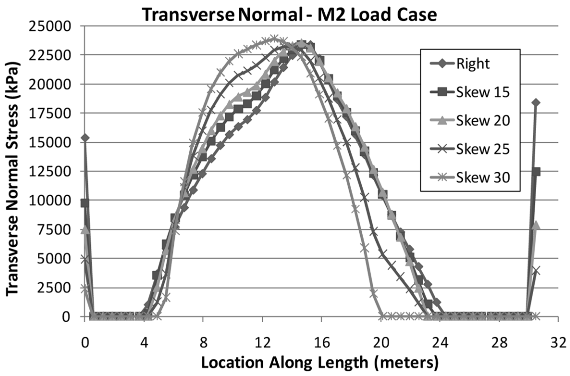

Fig. 12 Transverse axial stress (101.6-mm × 76.2-mm × 12.7-mm, zero diaphragms)

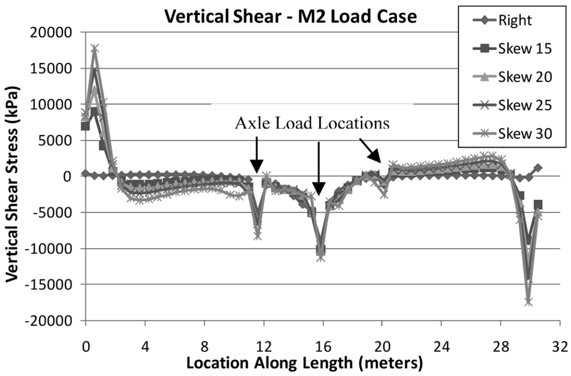

Fig. 13 Vertical shear stress (101.6-mm × 76.2-mm × 12.7-mm)

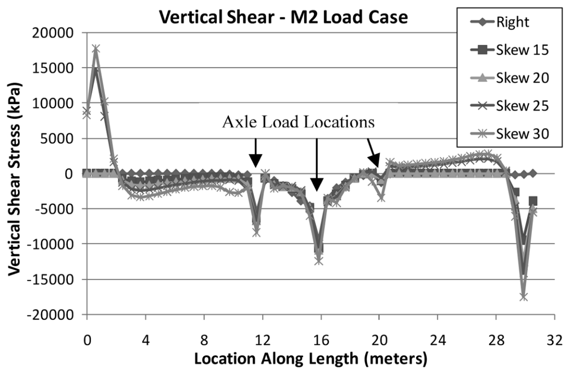

Fig. 14 Vertical shear stress (152.4-mm × 101.6-mm × 19.1-mm)

Fig. 13 shows the vertical shear stresses for the 101.6-mm × 76.2-mm × 12.7-mm steel plates spaced at 0.61-m (2-ft). The HL-93 truck axle load locations can be seen in the vertical shear stress data by the dips at the 11.58-m (38-ft), 15.85-m (52-ft), and 20.12-m (66-ft) locations. The dips in the vertical shear stress data at the 11.58-m (38-ft) and 15.85-m (52-ft) locations are larger than the dip at the 20.12-m (66-ft) location because the 142.34 kN (32 kips) axle loads exist at the 11.58-m (38-ft) and 15.85-m (52-ft) locations while the smaller 35.59 kN (8 kips) axle load exists at the 20.12-m (66-ft) location. The largest vertical shear stresses exist at the 0.61-m (2-ft) and 29.87-m (98-ft) location in Fig. 13 with a stress value of 18 MPa (2.61 ksi), which is well below the yield stress of A36 steel. Ma *et al.* (2007) also found that the maximum vertical shear force was found in the connectors located closest to the wheel loads as stated in their conclusions.

Fig. 14 shows vertical shear stresses for the 152.4-mm × 101.6-mm × 19.1-mm steel plates spaced at 0.61-m (2-ft). Comparing Fig. 14 to Fig. 13 shows that the larger steel plates provide limited advantage over the smaller 101.6-mm × 76.2-mm × 12.7-mm steel plates.

3.1.4 Effects of diaphragms

Diaphragms are used to transfer loads from one girder to the next. This section examines the effect of using one diaphragm and two diaphragms on bridge performance. Longitudinal spring elements are spaced at 0.61-m (2-ft) for both cases.

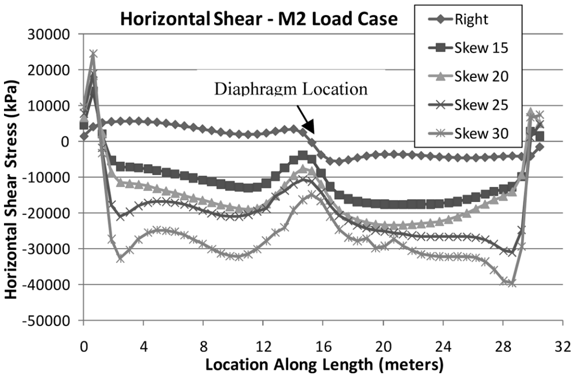

Fig. 15 Horizontal shear stress (0.61-m (2-ft spacing), one diaphragm)

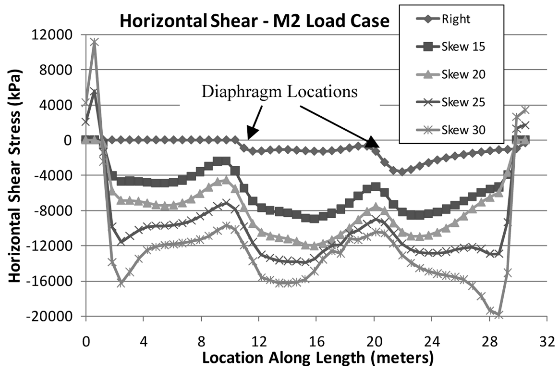

Fig. 16 Horizontal shear stress (0.61-m (2-ft spacing), two diaphragms)

The lack of a diaphragm (Fig. 12) has increased the transverse axial stress in the plates by a factor of 2.5 when comparing to the stress in Fig. 10 (one diagram). The single diaphragm at mid-span has a significant effect on the transverse behavior of the connectors.

Fig. 15 shows steel plate horizontal shear stresses for skew and right bridge geometries with one diaphragm at mid-span. The 101.6-mm × 76.2-mm × 12.7-mm steel plates along joint line D are located between Beam 4 and 5 seen in Fig. 2 and Fig. 5. Fig. 15 shows that as the skew angle in the bridge geometry increases, the absolute horizontal shear stress value also increases. The presence of the diaphragm at mid-span can be seen in Fig. 15 at the 15.24-m (50-ft) location along the length because the horizontal shear stress values are peaking in this location. The horizontal shear stresses increase in absolute value in the steel plates at the diaphragm location.

Fig. 16 shows steel plate horizontal shear stresses for skew and right bridge geometries with two diaphragms at 1/3 points along the length of the bridge. The 101.6-mm × 76.2-mm × 12.7-mm steel plates along joint line D are located between Beam 4 and 5 seen in Fig. 2 and Fig. 5. Examining Fig. 16, the diaphragm locations at 10.06-m (33-ft) and 20.12-m (66-ft) can be seen by the peaks in the horizontal shear stress values. When comparing Fig. 16 to Fig. 15, there are now two peaks signifying the location of the two diaphragms. Fig. 16 shows that as the skew angle increases in the bridge geometry, the absolute horizontal shear stress values also increase. Notice in Fig. 16 that the largest horizontal shear stress value exists in the bridge with a skew angle of 30° at the 28.65-m (94-ft) location along the length of the bridge. The stress value is 20 MPa (2.9 ksi). Notice at the same location for the same bridge configuration in Fig. 15 that the horizontal shear stress value is 40.7 MPa (5.9 ksi). This means the addition of two diaphragms at 1/3 points along the length of the bridge compared to one diaphragm at mid-span can reduce the horizontal shear stress up to 50%. This reduction in horizontal shear stress by adding more intermediate diaphragms was also found by Ma *et al.* (2007) as stated in their conclusions. None of the steel plates reached yielding when subjected to horizontal shear stress in this study.

3.1.6 Effects of rotational stiffness

The effects of rotational stiffness were examined considering the case of 101.6-mm × 76.2-mm × 12.7-mm steel plates modeled. As the adequacy of the rotational stiffness in Eq. (4) (a beam subjected to equal end moments) is unknown, two other cases of rotational stiffness, 4 times of that defined in Eq. (1) and zero rotational stiffness (thus no moment transferred), were investigated. Fig. 17 shows the transverse moment stresses in the steel along joint line D (Fig. 2) are shown in Fig. 17. The right bridge model has one diaphragm and is subjected to the M2 load case.

In Fig. 17, the largest stresses are transferred by the 101.6-mm × 76.2-mm × 12.7-mm steel plates modeled using the stiffness from Eq. (4). The steel plates modeled using the stiffness from Eq. (4) reduced by a factor of four have transverse moment stresses that are between those from the cases of stiffness determined from Eq. (4) and zero stiffness. The maximum stress of 17 MPa (2.5 ksi) in the steel plates is well below the 248 MPa (36 ksi) yield stress. That implies that the stresses induced are so small that it is unlikely that the stiffness increase would be large enough to cause stress problems.

3.2 Bridge deflections

Deflections for multiple bridge configurations subjected to the M2 load case were analyzed to understand the effects of welded shear connectors and diaphragm configurations on bridge deflections for skew and right bridge geometries. The bridge models have 101.6-mm × 76.2-mm × 12.7-mm steel plates spaced at 0.61-m (2-ft) with no diaphragms, one diaphragm at mid-span, or two diaphragms at 1/3 points along the length of the bridge, respectively. The deflections were taken from the top of Beam 4 along the longitudinal length at the quarter points.

Fig. 18 shows that the addition of one diaphragm at mid-span compared to no diaphragms for the right bridge model decreases the bridge deflection 40% at mid-span and 50% at the quarter points along the length of the bridge. The addition of two diaphragms at 1/3 points along the length of the bridge has virtually no effect on the bridge model deflection compared to one diaphragm at mid-span. When comparing Fig. 18 and Fig. 19, it can be seen that a skew angle of 30° exhibits about 15% more deflection at the mid-span and quarter point along the length of the bridge compared to a right bridge.

The differential deflection between adjacent girder deck flanges (SBHQ plate elements) was not investigated in this research. The differential deflection may contribute to the cracking in the overlay seen by the WSDOT (Hieber *et al.* 2005), which needs to be investigated in future work.

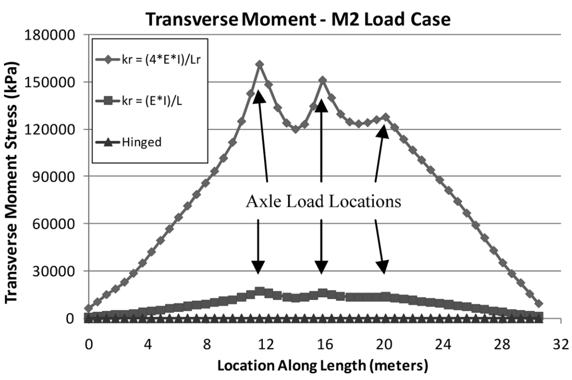

Fig. 17 Transverse moment stress – effects of rotational stiffness (0.61-m (2-ft) spacing)

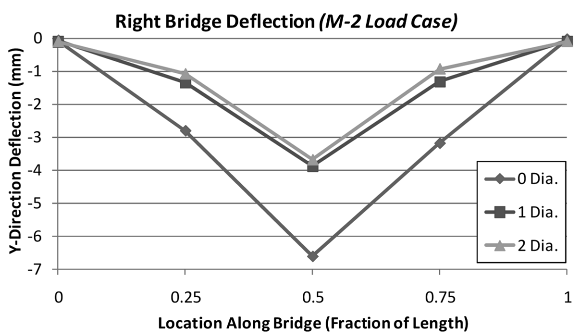

Fig. 18 Deflections of right bridge

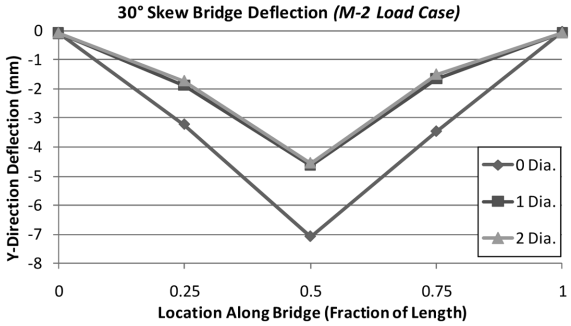

Fig. 19 Deflections of 30° skew bridge

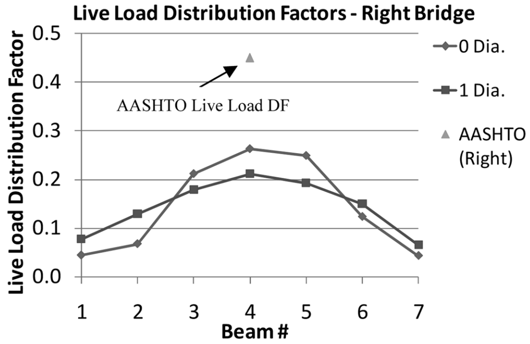

Fig. 20 Live load distribution factors for moment (0° skew)

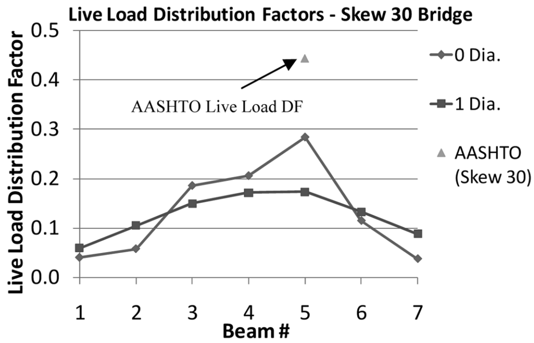

Fig. 21 Live Load distribution factors for moment (30° skew)

3.3 Live load distribution

Live load distribution in this study is based on moment at mid-span of each individual girder.

Fig. 20 and Fig. 21 show the live load distribution factors (DF) based on moment for right bridge geometries and bridge geometries with 30° skew. The 152.4-mm × 101.6-mm × 19.1-mm steel plates are spaced at 0.61-m (2-ft), and there was either no diaphragm or one diaphragm at mid-span. The models are subjected to the M2 load case. The AASHTO live load distribution factor (moment) for a DPPC girder was calculated and plotted for comparison (AASHTO 2007).

For the M2 load case, the truck axles are placed on the bridge such that Beams 3, 4, and 5 carry most of the live load, which can be seen in Fig. 5. The effects of the truck placement are evident in Fig. 20 because Beams 3, 4, and 5 have the largest live load distribution factor for bridge models with no diaphragm or one diaphragm at mid-span. The AASHTO live load distribution factor plotted for Beam 4 in Fig. 20 is conservative and almost 80% larger than the live load distribution factor from Beam 4 of the bridge model. Cai *et al.* (2002) along with Cai and Shahawy (2004) found that the AASHTO LRFD Bridge Design Specification (1998) produced conservative live load distribution factors for non-composite AASHTO girders. Notice that the addition of one diaphragm helps to distribute the load more evenly over the entire bridge (or reducing the live load distribution factors), as expected. Ma *et al.* (2007) also found this to be true as stated in their conclusions. The live load distribution factors from the bridge models with 15° of skew are not plotted because the live load distribution factors are similar to the ones seen in Fig. 20 for right bridge models.

Fig. 21 shows that the AASHTO live load distribution factor plotted for Beam 5 is conservative. The addition of one diaphragm compared to no diaphragms allows for more even distribution of loads from girder to girder. The addition of 30° of skew has some effect on live load distribution when comparing Fig. 21 to Fig. 20. Fig. 20 has a maximum live load distribution factor that is 10% to 15% larger than the maximum live load distribution factor in Fig. 21 showing that an increase in skew leads to a decrease in the live load distribution factors.

3.4 Future work

Future work may include the grout material stiffness in the spring elements to investigate the effects of the grout material on load transfer. Examining the differential displacement of the nodes connected to the spring elements to investigate reflective cracking by comparing data from the spring elements in the DPPC bridge models with actual field data should be considered. Bridges with skew angles larger than 30°, larger truck loads, and different sizes and spacing of the welded shear connectors should be considered as well.

4. Conclusions

The spring element modeling technique proposed in this study is intended to demonstrate the feasibility of such a method for evaluating the performance of joint connections for DPPC girder bridges. Spring elements were used to model welded shear connectors in right and skew bridges to investigate joint connection behavior, effects of connector spacing, effects of rotational rigidity, effects of skew angle, bridge deflections, and live load distribution factor for moment in the preliminary study. The method is simplified compared to other similar methods (e.g., Jones and Boaz 1986). Nevertheless, the method has the ability to represent a range of connector types, with a potential to include the contribution of the grout material placed along the longitudinal joints. The spring elements can be a useful tool for modeling the welded shear connectors and for examining implications for the design of welded shear connectors for rapid bridge replacement.

References

American Association of State Highway and Transportation Officials (AASHTO) (2006), *Interim AASHTO LRFD Bridge Design Specifications*, 3rd edition, Washington, D.C.

American Association of State Highway and Transportation Officials (AASHTO) (2007), *AASHTO LRFD Bridge Design Specifications*, 4th edition, Washington, D.C.

American Society of Civil Engineers (ASCE) (2009), "Report Card for America's Infrastructure", < http://www.asce.org/reportcard/2009/grades.cfm>

Boresi, A.P. and Schmidt, R.J. (2002), *Advanced Mechanics of Materials*, John Wiley & Sons Publishing.

Cai, C.S. and Shahawy, M. (2004), "Predicted and measured performance of prestressed concrete bridges", *J. Bridge Eng.,* **9**(1), 4-13.

Cai, C.S., Shahawy, M. and Peterman, R.J. (2002), "Effect of diaphragms on load distribution in prestressed concrete bridges", *Transportation Research Record*, 1814, Transportation Research Board, Washington, D.C.

Chaudhury, S. and Ma, Z. (2004), "Effect of connections between adjacent units on decked precast/prestressed

concrete girder bridges", *PCI National Bridge Conference,* Atlanta, Georgia, February.
Gergely, J., Overcash, G.L., Mock, J.B., Clark, C.M. and Bailey, K.G. (2007), "Evaluation of design and construction of HPC deck girder bridge in stanly county, North Carolina", Report No. FHWA/NC/2006-18, Univ. of North Carolina at Charlotte, Civil Engineering Dept., Charlotte, NC.
GTStrudl (2006), *GTStrudl Version 29*, Georgia Institute of Technology, Atlanta.
Hieber, D.G., Wacker, J.M., Eberhard, M.O. and Stanton, J.F. (2005), *State-of-the-Art Report on Precast Concrete Systems for Rapid Construction of Bridges*, Washington State Transportation Center (TRAC), Univ. of Washington, Seattle, Washington.
Jones, H.L. and Boaz, I.B. (1986), "Skewed discretely connected multi-beam bridges", *J. Struct. Eng.,* **112**(2), 257-272.
Ma, Z.J., Chaudhury, S., Milliam, J.L. and Hulsey, J.L. (2007), "Field test and 3D FE modeling of decked bulb-Tee bridges", *J. Bridge Eng.,* **12**(3), 306-314.
Michigan Department of Transportation (MDOT) (2005), "Bridge Design Manual", <http://http://mdotwas1.mdot.state.mi.us/ public/design/ englishbridgemanual/>
Millam, J.L. and Ma, Z. (2005), "Single lane live load distribution factor for decked precast, prestressed concrete girder bridges", *Transportation Research Record*, 1928, Transportation Research Board, Washington, D.C.
Pipkorn, T.M. (2006), "Development of rapid construction solutions using prefabricated prestressed concrete systems", MS thesis, Michigan Technological Univ., Houghton, MI.
Precast/Prestressed Concrete Institute (PCI) (2007), *State of the Art of Precast/Prestressed Adjacent Member Bridges,* Chicago, IL.
PSBeam (2000), *PSBeam Version 2.00*, Eriksson Technologies, Inc., Temple Terrace, FL.
Smith, M.Z. (2007), "Analysis of longitudinal joint connections for decked precast prestressed concrete girder bridges", MS thesis, Michigan Technological Univ., Houghton, MI.